





Article

A Tesla Valve as a Micromixer for Fe₃O₄ Nanoparticles

Christos Liosis ¹, George Sofiadis ², Evangelos Karvelas ^{2,3}, Theodoros Karakasidis ³ and Ioannis Sarris ^{2,*}¹ Department of Civil Engineering, University of Thessaly, 38334 Volos, Greece² Department of Mechanical Engineering, University of West Attica, 12243 Athens, Greece³ Condensed Matter Physics Lab, Department of Physics, University of Thessaly, 35100 Lamia, Greece

* Correspondence: sarris@uniwa.gr; Tel.: +30-6941672950

Abstract: A large number of microfluidic applications are based on effective mixing. In the application of water purification, the contaminated water needs to be effectively mixed with a solution that is loaded with nanoparticles. In this work, the Tesla valve was used as a micromixer device in order to evaluate the effect of this type of geometry on the mixing process of two streams. For this reason, several series of simulations were performed in order to achieve an effective mixing of iron oxide nanoparticles and contaminated water in a duct. In the present work, a stream loaded with Fe₃O₄ nanoparticles and a stream with contaminated water were numerically studied for various inlet velocity ratios and initial concentrations between the two streams. The Navier–Stokes equations were solved for the water flow and the discrete motion of particles was evaluated by the Lagrangian method. Results indicate that the Tesla valve can be used as a micromixer since mixing efficiency reached up to 63% for $V_p/V_c = 20$ under various inlet nanoparticles rates for the geometry of the valve that was used in this study.

Keywords: tesla valve; Fe₃O₄ nanoparticles; micromixer; water purification; CFD; DEM



Citation: Liosis, C.; Sofiadis, G.; Karvelas, E.; Karakasidis, T.; Sarris, I. A Tesla Valve as a Micromixer for Fe₃O₄ Nanoparticles. *Processes* **2022**, *10*, 1648. <https://doi.org/10.3390/pr10081648>

Academic Editor: Avelino Núñez-Delgado

Received: 29 July 2022

Accepted: 16 August 2022

Published: 19 August 2022

Publisher's Note: MDPI stays neutral with regard to jurisdictional claims in published maps and institutional affiliations.



Copyright: © 2022 by the authors. Licensee MDPI, Basel, Switzerland. This article is an open access article distributed under the terms and conditions of the Creative Commons Attribution (CC BY) license (<https://creativecommons.org/licenses/by/4.0/>).

1. Introduction

Mixing and separation of nanoparticles is of great interest in the scientific community due to the variety of applications that may be useful. This arises from the diminutive scale of the flow channels in microfluidic systems, which increases the surface-to-volume ratio [1]. The aim of microfluidic devices is to achieve rapid mixing with high mixing efficiency by enhancing the diffusion effect between the different species flows [2]. Passive micromixing systems are defined based on their geometry and any natural flow features that arise [3]. These microfluidic devices do not use any external actuator to drive the fluids or guide the particles in the fluid [4]. In micromixers, the flow rates and the regime of the fluids are significantly low and laminar, respectively. Thus, this indicates that the fluid flows in parallel layers with no disruption between the layers and the mixing of the fluids is mainly dependent on diffusion with a very low mixing efficiency [5].

Computational fluid dynamics (CFD) and micromixers may offer a solution to contaminated water from heavy metal ions [6–8]. The majority of experimental water purification methods involve magnetic nanoparticles due to their physicochemical properties [9]. Due to their spatial confinement, large surface area–volume ratio, and small size [10,11], bare or modified Fe₃O₄ nanoparticles are most commonly used. Among other iron phases, maghemite and magnetite stand out due to strong magnetic moments and some structural features [12]. Several parameters from experimental data, such as monodispersity [13,14] and particle diameter [12,15], are embedded in the simulations for a more realistic approach. In addition, nanofluids' physical characteristics vary with the alteration in nanoparticles in terms of type, size, shape, base liquid, and volume fraction [16,17]. The combination of micromixers and computational fluid dynamics, and the progress of nanotechnology, may define a solution for heavy metal adsorption in water solutions [18].

Micromixing devices often utilize complex architectures to achieve high mixing performance [19]. A 1920 patent by Tesla, named ‘valvular conduit’, has recently attracted scientific interest in the field of fluidics, and can lead to applications in fluidic mixing [20]. In order to investigate the purification of water through simulations, Tesla’s valve used as a micromixer device has been promoted as a possible solution. Unbalanced collision-based micromixers, such as the Tesla micromixer, are usually dependent on the asymmetric structure of the channel or the different flow rate of the fluids [5]. A huge variety of Tesla’s valve geometries already exists. Related works that use the Tesla valve as a micromixer achieve a mixing efficiency of up to 96.47% [21]. Generally, the factors affecting the mixing efficiency are the Reynolds number (Re) and geometric parameters when designing and evaluating micromixers [22]. Re varies from 0.05 to 100 [22,23] for Tesla micromixers, whereas the geometric parameters are more chaotic in terms of dimension and contact angle (θ°). The dimensions of one Tesla valve vary from [24] μm to [21] mm, and the contact angle varies from 30° [21] to 55° [23]. In addition, the determinant is the number of Tesla micromixers, at a given mixing efficiency, which are usually used in series. The total length is related to the number and the dimension of the Tesla units being used. Using twenty units [25] the total length reaches up to 6 mm, whereas using three units [23] the length reaches up to 16.04 mm. As the number of Tesla micromixers increases, mixing efficiency is significantly increased; however, the mixing efficiency is stabilized after several additions of micromixers. It should be noted that the Tesla valve can be used in normal or/and inverse flows as a micromixer. Table 1 shows the characteristics of related works and the present study.

Table 1. Characteristics and mixing efficiency of different Tesla-type micromixers.

Number of Tesla Micromixers	Direction of Flow	Contact Angle θ°	Reynolds Number (Re)	Mixing Efficiency	Ref.
20			0.1	0.78	[24]
10			100	0.950	[26]
20			100	0.97	[25]
6			40	0.702	[22]
3	Inverse	30	1	0.953	[23]
8	Inverse	30	52.5	0.9647	[21]
2	Normal	30	0.62	0.63	present study

In the present study, a passive micromixer was simulated where the heavy metal-contaminated water stream and the freshwater stream loaded with nanoparticles were inserted in a microfluidic duct. Heavy metal can be captured by nanoparticles through chemical reactions under various initial conditions [10]. Numerical simulations were performed in order to evaluate the initial inlet rate of Fe_3O_4 nanoparticles and the inflow effect on the particle distribution in the mixing process.

The discrete element method was used for first time in order to simulate the nanoparticles’ trajectories inside the Tesla valve. The location of each nanoparticle and the distribution of the nanoparticles, which are coated with the appropriate substances in order to bind the heavy metals, is crucial for the optimization of the mixing process. Therefore, using the present method, more robust conclusions can be extracted for the mixing procedure than by using only diffusion models. In this context, specific actions can be taken for the optimization of the mixing process.

The methodology for water flow and particle motion simulation is described in Section 2. The results of the mixing performance are discussed in Section 3. The results of the simulations are presented in Section 4, and conclusions are summarized in Section 5.

2. Materials and Methods

The present numerical model was validated against the experimental results from the reference [27]. In this previous study [27], Fe_3O_4 particles were both experimentally investigated and numerically simulated for the evaluation of the particles’ velocity in

microchannels. The numerical model can successfully predict the mean velocity of the particles inside the microchannels, as depicted in Table 2. In addition, the results of the present numerical model present great qualitative and quantitative agreement compared to the experimental results and other numerical models, as depicted in Table 2.

Table 2. Comparison of the present results against experimental and simulation results from Ref. [27].

Case	Mean Velocity ($\mu\text{m/s}$)	Std Velocity ($\mu\text{m/s}$)
Experiment, Ref. [27]	7.5	1
Numerical, Ref. [27]	9	2
Present study	8.3	1.4

Investigation was carried out of nanofluid flow through a microchannel subjected to various effects [11]. The slow water flow in the micromixer duct was expected to be laminar and steady-state. The selection among the different Tesla mixing units was made with the criterion that the specific geometry has been studied less compared to those in Table 1.

The inlet and the outlet of the micromixer was a squared cross-section with height and width of $W = H = 10^{-4}$ m. The angle of $\theta = 30^\circ$ and the length ratio of $L_1/L_2 = 2$ were selected from an existing Tesla structure [21]. In addition, properties of Fe_3O_4 were numerically embedded in the simulations. The values of these properties found from the literature correspond to a density equal to 5180 kg/m^3 [28], Poisson's ratio equal to 0.31, and Young's modulus of $200 \times 10^9 \text{ Pa}$ [29]. Determination of the selection of nanoparticle diameters was based on Chang and Chen [30]. Successful removal of heavy metal ions was achieved within 1 min for monodisperse Fe_3O_4 magnetic nanoparticles having a mean diameter size of 13.5 nm. In addition, an even lower time (30 s) of adsorption equilibrium was achieved [31], which is encouraging for the mixing length of the microfluidic devices. The two water streams enter the micromixer from different inlets, are mixed, and the leave the domain from the common outlet, as shown in Figure 1.

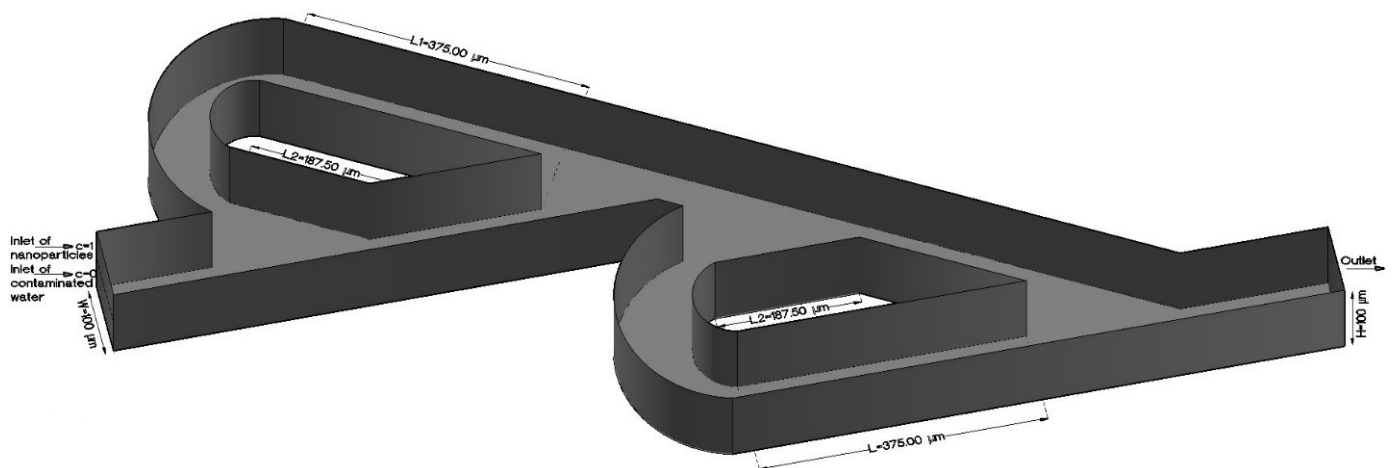


Figure 1. Micromixer geometry and nanoparticles, contaminated water inlets, and outlet flow directions.

The incompressible Navier–Stokes equations are solved in the Eulerian frame, for the pressure p and velocity u , together with a model for the discrete motion of particles in a Lagrangian frame. Governing equations of the fluid phase are given by [6]:

$$\nabla \cdot u = 0 \quad (1)$$

$$\frac{\partial u}{\partial t} + u \cdot \nabla u = -\nabla p + \nu \nabla^2 u \quad (2)$$

where t is time and ν the kinematic viscosity of the water. Details of the numerical models, force, and moment terms used in the equations may be found in Refs. [8,32]. The motion equations of each single particle in the discrete frame are based on the Newton law and may be presented as follows:

$$m_i \frac{\partial u_i}{\partial t} = F_{nc,i} + F_{tc,i} + F_{drag,i} + F_{grav,i} \quad (3)$$

$$I_i \frac{\partial \omega_i}{\partial t} = M_{drag,i} + M_{con,i} \quad (4)$$

where the index i stands for the i th particle with diameter d_i ; u_i and ω_i are its transversal and rotational velocities, respectively, and m_i is its mass. The mass moment of inertia matrix is I_i and the terms $\partial u_i / \partial t$ and $\partial \omega_i / \partial t$ correspond to the linear and angular accelerations, respectively. $F_{nc,i}$ and $F_{tc,i}$ are the normal and tangential contact forces, respectively. $F_{drag,i}$ represents the hydrodynamic drag force and $F_{grav,i}$ is the total force due to buoyancy. $M_{drag,i}$ and $M_{con,i}$ are the drag and contact moments, respectively.

The Reynolds number (Re) is defined as $Re = \frac{\rho V D}{\mu} = \frac{V D}{\nu}$, where $\rho = 10^3 \text{ kg/m}^3$ is density of the fluid, μ indicates the fluid dynamic viscosity coefficient, and $\nu = 10^{-6} \text{ m}^2/\text{s}$ is the kinematic viscosity of the fluid. D is the characteristic linear dimension, which is equal to the hydraulic diameter (D_h), for square inlet ducts $D_h = \frac{4 \cdot A}{O}$, where A (m^2) is the cross-section area of the duct and O (m) is the wetted perimeter. In this case, D_h was found to be equal to $W = H = 10^{-4} \text{ m}$. Finally, V is the maximum velocity developed inside the duct. Re was found to be 0.62, 0.63, and 0.1 for $V_p/V_c = 20$, $V_p/V_c = 10$, and $V_p/V_c = 1$, respectively, in the present work.

The OpenFoam platform is used for the calculation of the flow field and the uncoupled equations of particle motion [33,34]. The simulation process reads as follow: initially, the fluid flow is found using the incompressible Navier–Stokes equations and the pressure correction method. Upon finding the flow field, pressure, and velocity, the motion of particles is evaluated by the Lagrangian method. The equations are evolved in time by Euler’s time marching method. An unstructured computational grid composed of 96,881 (tetrahedra) cells was used here, as shown in Figure 2, which is adequate for the low Reynolds number of the flow. However, the selectivity of the mesh based on the importance of geometric and operating parameters was assessed to obtain a significant number of computational predictions in a reasonable time without compromising the validity of the results [19].

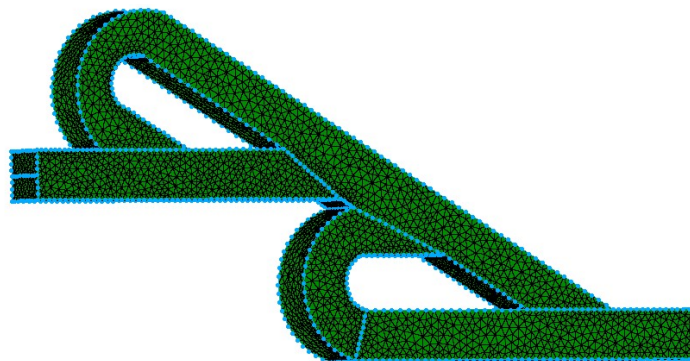


Figure 2. Micromixer mesh.

In the current project, the mixing efficiency was evaluated. The mixing efficiency (n) is calculated as follows [35]:

$$n = 1 - \sqrt{\frac{\sigma_C^2}{\sigma_{\max}^2}} = 1 - \frac{\sqrt{\frac{1}{N-1} \sum_{i=1}^N (C_i - \bar{C})^2}}{\bar{C}(1 - \bar{C})} \quad (5)$$

where σ_{\max}^2 is the square of the maximum possible variance and σ_C^2 is defined by N , which is the number of sampling points ($N = 16$ for present work) and $N - 1$ is given by applying Bessel's correction; c_i is the point concentration; and \bar{C} is the optimal concentration. Moreover, two inlet concentrations are defined as $C = 0$ and $C = 1$. Mixing efficiency (n) ranges between 0 and 1, which represent no mixing and fully mixed, respectively. In this way, mixing efficiency can be characterized on the basis of numerical simulations of the tracer concentration field [35].

The mixing cost (mc) is defined as the ratio of the mixing efficiency to the pressure drop in the microchannel and is given by [19,36]:

$$Mc = \frac{\Delta P}{n} \quad (6)$$

where ΔP is the pressure drop and n is the mixing efficiency (%). The units of the mixing cost are Pa/%, and this measures the pressure needed in the device to obtain efficiency of just 1% and make the fluids flow at the specific Re [36].

3. Results

The simulations performed focused on different velocity ratios of the contaminated water (V_c) and the nanoparticle solution (V_p) streams, and nanoparticle diameters, for the investigation of mixing performance. Simulation parameters and the boundary conditions are tabulated in Table 3.

Table 3. Parameters during the simulations.

Simulation Parameters			
inlet and outlet dimensions (m)	Height (H) = Width (W) = 10^{-4}		
diameter of Fe_3O_4 nanoparticles (nm)	13.5, 27		
inlet rate of Fe_3O_4 nanoparticles	500/s, 1000/s, 3000/s		
Boundary conditions			
(V_c) contaminated water (m/s)	0.0005, 0.00005, 0.000025	zero gradient	
(V_p) nanoparticles (m/s)	0.0005	zero gradient	
outlet	zero gradient	0	
walls	0	zero gradient	

Simulations were divided into two main parts, which were the evaluation of the velocity and pressure field, and the particle distribution into the micromixer. Initially, from the variance in the fluids, a cross-section of the microchannel parallel to the flow direction [37] was evaluated for $V_p/V_c = 20$, $V_p/V_c = 10$, and $V_p/V_c = 1$. Under higher velocity ratios, the velocity field decreases inside the duct, which arises from the comparison of the selected velocity ratios. This decrease is not proportional to the increase in the velocity ratio. The rate of nanoparticles remained constant for the entire simulations. Part of the present results are visualized in Figure 3. From simulation results shown in Figure 3a–c, the inlet rate was equal to 1000 Fe_3O_4 nanoparticles per second in the upper half inlet of the micromixer. Hence, the only difference between 3a, 3b, and 3c is the inlet velocity ratio. Under $V_p/V_c = 20$ (3a) and $V_p/V_c = 10$ (3b), the distribution is satisfied, as observed from the beginning of the micromixer. In the first loop (upper part of the micromixer), the distribution of the nanoparticles is uniform, whereas in the second loop (lower part of the micromixer), the distribution is not satisfied. Near the common outlet, a very satisfying distribution is observed. It should be noted that, in the present simulations, only two Tesla valves were used in series compared to previous works, as shown in Table 1. However, under $V_p/V_c = 1$ (3c), no mixing was observed inside the whole length of the micromixer. Moreover, the results were almost identical when the inlet rates of Fe_3O_4 nanoparticles (diameter = 13.5 nm) were either 1000/s or 3000/s for both velocity ratios.

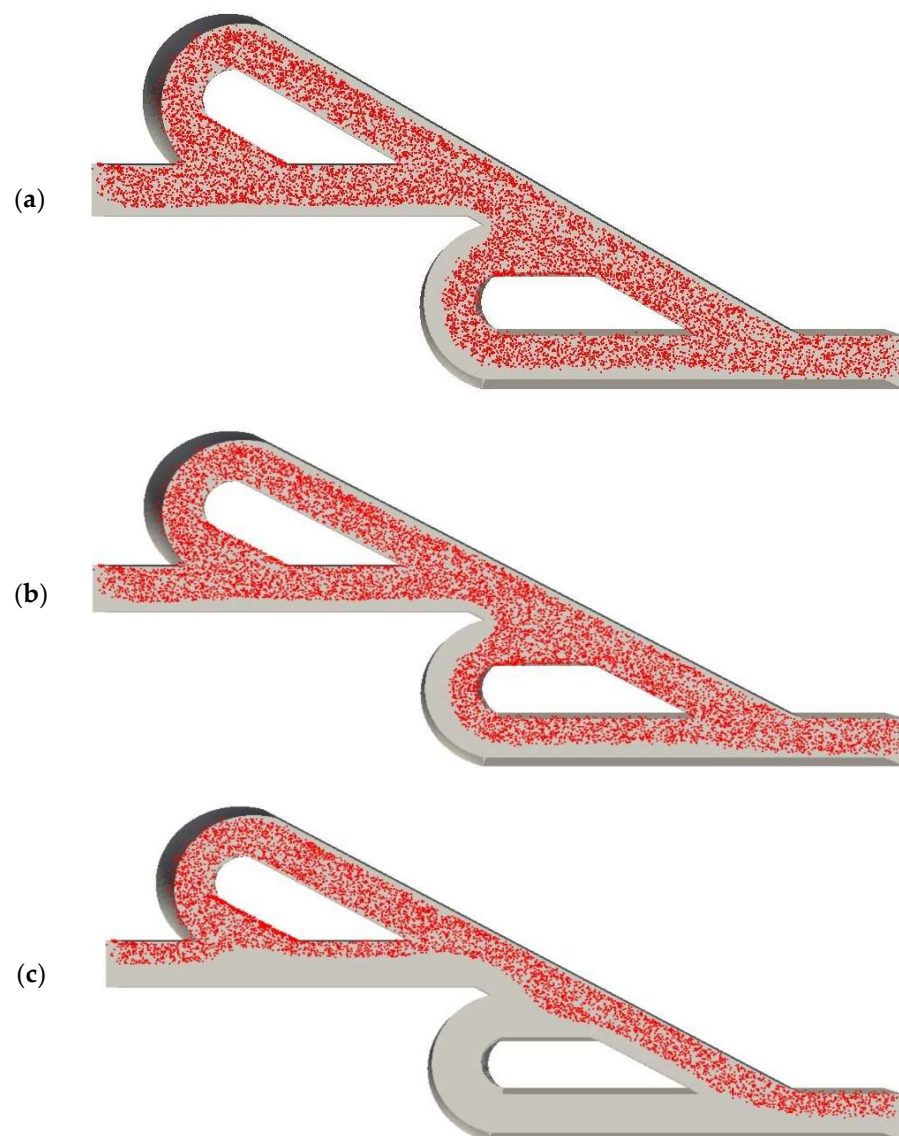


Figure 3. Distribution of nanoparticles (diameter = 13.5 nm) in the micromixer for a rate equal to 1000 nanoparticles per second under (a) $V_p/V_c = 20$, (b) $V_p/V_c = 10$, and (c) $V_p/V_c = 1$.

Under $V_p/V_c = 1$, no mixing was observed from the visualization of the simulations for all inlet rates. Thus, only results from $V_p/V_c = 10$ and $V_p/V_c = 20$ were quantified. Figure 4 shows the mixing efficiency for various inlet rates. The efficiency was calculated using Equation (5) and the number of sample points (N) was selected to be equal to 16. These “sample points” were actually volumes that occurred due to division of the height (H) and the width (W) into four equal sections of 25 μm . Moreover, the length of each N was equal to 100 μm . It should be noted that the volume of N should not affect the mixing efficiency since the nanoparticles are in a steady condition in the micromixer. In order to evaluate this hypothesis, the efficiency was calculated for two different volumes of N and the mixing performance showed no significant change.

It was found that the inlet rates of nanoparticles have a significant role in mixing efficiency. Under the same inlet ratios, the increase in inlet rates coincides with the increase in efficiency. Moreover, the difference in mixing efficiency between 500 and 3000 particles per second was about 20% for $V_p/V_c = 10$, while the increase in the inlet ratio difference dropped to 9%. The mixing efficiency of this specific micromixer was over 63% for $Re = 0.62$.

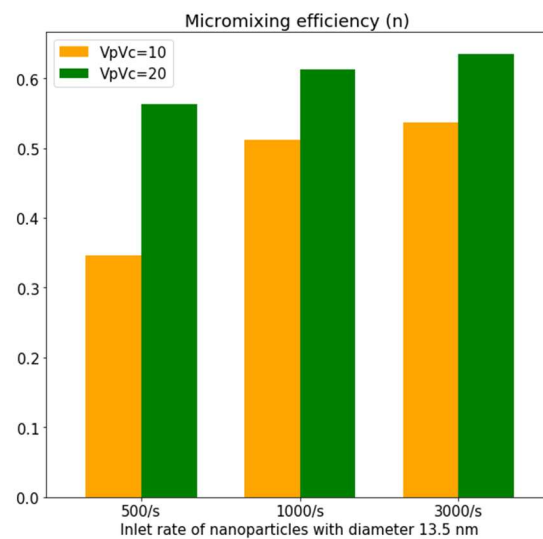


Figure 4. Mixing efficiency for $V_p/V_c = 10$ and $V_p/V_c = 20$ under inlet rates equal to 500, 1000, and 3000 nanoparticles per second.

The mixing cost for $V_p/V_c = 20$ and $Re = 0.62$ calculated from Equation (6) using the micromixer achieved a better mixing performance. Under an inlet rate equal to 500 nanoparticles per second, ΔP was found to be 0.840 Pa while mixing performance was 56.31%; thus, the mixing cost was 1.49 Pa/%. By comparison, when the inlet rate was increased to 1000 nanoparticles per second, ΔP was found to be 0.834 Pa while the mixing performance was 61.22%. Thus, the mixing cost was calculated to be 1.36 Pa/%. Finally, under the inlet rate equal to 3000 nanoparticles per second, ΔP was found to be 0.843 Pa while the mixing performance was 63.43%; hence, the mixing cost was 1.33 Pa/%.

The streamlines of the duct are presented in Figure 5 under all the selected velocity ratios. In Figure 5a, the streamlines are visualized for a velocity ratio equal to $V_p/V_c = 20$, where streamlines are curved before the first loop due to the high velocity difference between the two inlets. Hence, the mixing is strongly dependent on the velocity ratio and no recirculation occurs near the duct entrance. As the velocity ratio is decreased to $V_p/V_c = 10$ (Figure 5b), the above phenomenon is less intense. Moreover, when the velocity of both streams is equal (Figure 5c), the phenomenon does not appear, and thus no mixing is achieved, as also shown in Figure 3c.

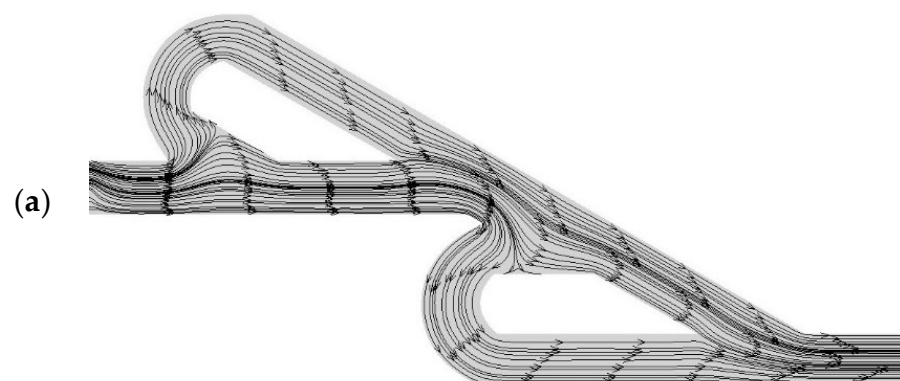


Figure 5. Cont.

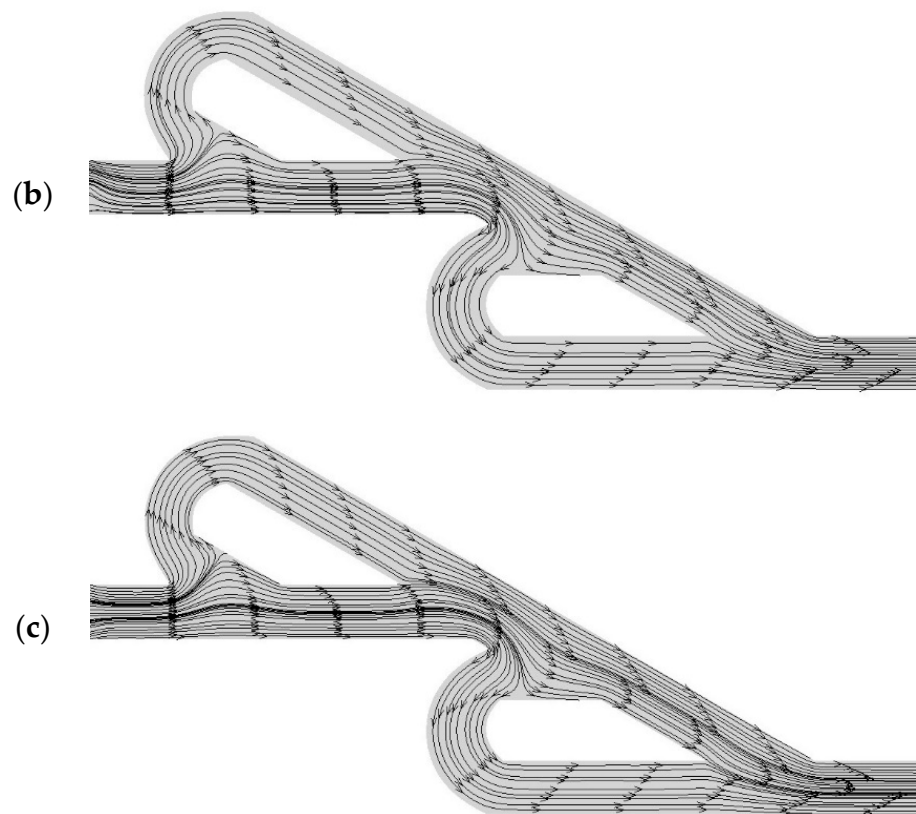


Figure 5. Streamlines into the micromixer for velocity ratios equal to (a) $V_p/V_c = 20$, (b) $V_p/V_c = 10$, and (c) $V_p/V_c = 1$.

In addition, the streamlines under $V_p/V_c = 20$ for a new geometry where the inlet is the longest ($200\ \mu\text{m}$) compared to the initial geometry was investigated. This expansion took place in order to examine if the phenomenon that arose in Figure 5 depends on the inlet length of the micromixer. The visualization (Figure 6) of the streamlines shows that phenomenon is independent of the inlet length, although the minor differences are in the range of statistical error. Hence, the mixing performance is strongly related to the inlet velocity ratios of the expanded micromixer.

Further simulations with a diameter increase in nanoparticles were performed for nanoparticles having a diameter set to $27\ \text{nm}$, which is double that of the above simulations. The difference in mixing efficiency between different diameters of nanoparticles for various inlet conditions is presented in Figure 7. The mixing difference is imperceptible, as shown below. For lower inlet rates, the difference is slightly lower. Moreover, for higher inlet velocity ratios, the difference is minimized.

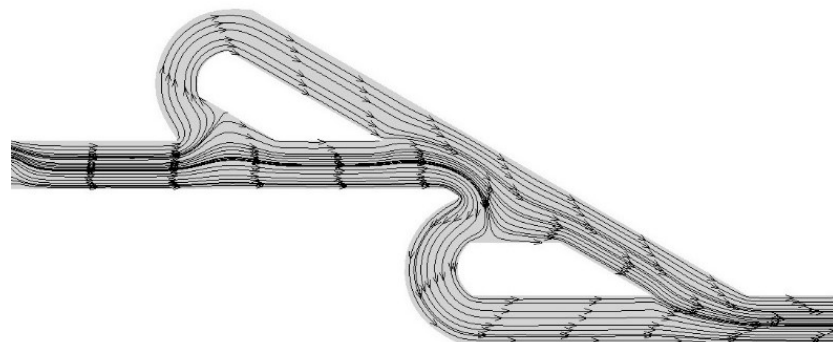


Figure 6. Streamlines into the micromixer for the velocity ratio equal $V_p/V_c = 20$ for the longest inlet.

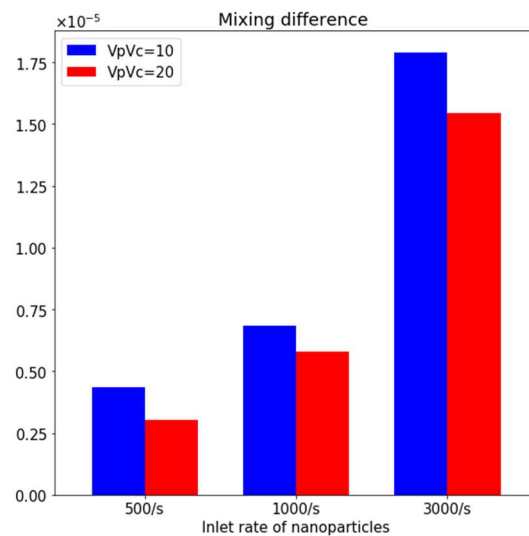


Figure 7. Mixing differences between different diameters of nanoparticles under inlet velocity ratios $V_p/V_c = 10$ and $V_p/V_c = 20$ and inlet rates equal to 500, 1000, and 3000 nanoparticles per second.

4. Discussion

Micromixer devices are involved in applications for water purification of heavy metals ranging from determination of heavy metal traces [38] to enhancing reactions [39]. Here, the basic principle is to achieve high mixing performance to enable application of the adsorption mechanism. Observations from the existing results show that, as V_p/V_c increases, mixing is achieved independently of the rates of Fe_3O_4 nanoparticles. Secondly, mixing is not achieved for all the cases with $V_p/V_c = 1$, under all the selected rates of Fe_3O_4 nanoparticles and diameters. Additionally, the inlet velocity ratio seems to be crucial for the mixing inside micromixers, either for the simplest geometries [32] with or [6] without an external magnetic field, or for more complicated geometries such as in the present work. The rate of Fe_3O_4 nanoparticles is the second factor that was investigated in the present work. Under both velocity ratios for all inlet rates, the outcomes from visualization and quantification lead us to conclusion that inlet rates affect the mixing efficiency of the micromixer.

Comparing the outcomes of the present work with previous studies (Table 1) of Tesla valve geometry, interesting similarities in the results were found. Initially, the difference between the mixing efficiency of Weng et al. [21] and the present work, which share basic parameters, such as the angle of $\theta = 30^\circ$ and the length ratio of $L_1/L_2 = 2$, is due to the number of Tesla valves in series (8). Comparing the mixing performance after the second Tesla valve, Weng et al. [21] found a mixing performance equal to 51.93%, which is lower than the current results. Thus, scaling down does not affect the successful micromixer geometry, and the results are also close enough to those of Weng et al. [21].

Moreover, researchers have explored several alterations to Tesla geometry. The geometry of Hossain et al. [22] employs a T-junction inlet with six serial valves and results in a mixing efficiency of 70.02%. Unfortunately, we could not directly compare our results with these because Hossain et al. [22] do not provide information about the mixing efficiency after the second Tesla valve. The mixing efficiency of the present work (63%) is close to that of Hossain et al. [22]. Another variation in the geometry uses a Y-junction inlet with 20 serial valves, as presented by Bhagat et al. [24]. This geometry achieved a mixing efficiency of 78% and has many similarities with the previous geometry. As in the previous case, the comparison could not be made directly but the difference in the mixing efficiency is obvious, and is probably due to the number of Tesla valves. Another micromixer was introduced by Wang et al. [23] that achieved a mixing efficiency up to 95.3% for three Tesla units. Efficiency for one valve (68.9%) is comparable with that in the present work, whereas using two valves exceeds our performance, achieving efficiency of 88.2%. Another high performance micromixer (97%) using a T-junction inlet and 10 unit pairs of valves

was introduced by Yang et al. [25]. Finally, the common characteristic between the above micromixers is that they are based on the micromixer of Hong et al. [26], which achieved a mixing efficiency of 95% for a T-shape inlet.

As is made clear by comparing the above mixing efficiencies, it is quite difficult to directly compare the diffusion and discrete models. This difficulty is due to several factors, such as different geometries and initial conditions. However, the work presented by Weng et al. [21] shares the same geometry (with only minor differences). Thus, we may be able to compare the models. The discrete model has better mixing efficiency than the diffusion model in the specific comparison. Although no clear conclusion can be drawn from a single comparison, we can nevertheless accept it as an indication.

5. Conclusions

In the present work, the Tesla valve geometry is used as a micromixer. In order to achieve high mixing efficiency performance of Fe_3O_4 nanoparticles inside the micromixer, several factors were investigated. Emphasis was placed on inlet velocity ratios and inlet rates of nanoparticles, and forward flow was selected for the simulations. Outcomes from the visualization of the simulations demonstrate that, when the velocity was equal to $V_p/V_c = 20$, nanoparticles were spread uniformly inside the micromixer (with the exception of the lower loop). The mixing efficiency achieved for $\text{Re} = 0.62$ and two Tesla units was 63%. Moreover, nanoparticles occupied a large percentage of the height and the width of the micromixer near the common exit. In addition, the quantification of results exhibited a significant role of inlet rates in determining mixing efficiency for lower velocity ratios. Additionally, the crucial factor for mixing efficiency was the velocity ratio, which acquired a decisive role as it increased. The increase in the nanoparticle's diameter from 13.5 to 27 nm had an insignificant impact on mixing performance, although more simulations need to be performed for different diameters. Further investigation of mixing performance is needed either for reverse flow or the addition of Tesla valves in series, according to the bibliography. Since the results are encouraging by comparison to the mixing performance of related works, this simplified model will be upgraded. An external magnetic field for investigation of a micromixing enhancement and adsorption model will be embedded in the model.

Author Contributions: Conceptualization, C.L.; methodology, E.K. and G.S.; software, C.L.; validation, C.L. and I.S.; formal analysis, C.L.; investigation, E.K.; resources, T.K.; data curation, T.K.; writing—original draft preparation, C.L.; writing—review and editing, I.S.; visualization, G.S.; supervision, T.K.; project administration, T.K. All authors have read and agreed to the published version of the manuscript.

Funding: European Regional Development Fund: MIS 5047244.

Data Availability Statement: Not applicable.

Acknowledgments: This work is partially supported by the project “ParICT_CENG: Enhancing ICT research infrastructure in Central Greece to enable processing of Big data from sensor stream, multimedia content, and complex mathematical modeling and simulations” (MIS 5047244) which is implemented under the Action “Reinforcement of the Research and Innovation Infrastructure”, funded by the Operational Programme “Competitiveness, Entrepreneurship and Innovation” (NSRF 2014–2020) and co-financed by Greece and the European Union (European Regional Development Fund).

Conflicts of Interest: The authors declare no conflict of interest.

References

1. Lee, C.Y.; Fu, L.M. Recent Advances and Applications of Micromixers. *Sens. Actuators B Chem.* **2018**, *259*, 677–702. [[CrossRef](#)]
2. Lee, C.Y.; Chang, C.L.; Wang, Y.N.; Fu, L.M. Microfluidic Mixing: A Review. *Int. J. Mol. Sci.* **2011**, *12*, 3263–3287. [[CrossRef](#)] [[PubMed](#)]
3. Green, J.; Holdø, A.; Khan, A. A Review of Passive and Active Mixing Systems in Microfluidic Devices. *Int. J. Multiphys.* **2007**, *1*, 1–32. [[CrossRef](#)]

4. Bayareh, M.; Ashani, M.N.; Usefian, A. Active and Passive Micromixers: A Comprehensive Review. *Chem. Eng. Process. Process Intensif.* **2020**, *147*, 107771. [[CrossRef](#)]
5. Cai, G.; Xue, L.; Zhang, H.; Lin, J. A Review on Micromixers. *Micromachines* **2017**, *8*, 274. [[CrossRef](#)]
6. Karvelas, E.; Liosis, C.; Karakasidis, T.; Sarris, I. Mixing of Particles in Micromixers under Different Angles and Velocities of the Incoming Water. *Proceedings* **2018**, *2*, 577. [[CrossRef](#)]
7. Liosis, C.; Karvelas, E.G.; Karakasidis, T.; Sarris, I.E. Numerical Study of Magnetic Particles Mixing in Waste Water under an External Magnetic Field. *J. Water Supply Res. Technol.* **2020**, *69*, 266–275. [[CrossRef](#)]
8. Karvelas, E.; Liosis, C.; Benos, L.; Karakasidis, T.; Sarris, I. Micromixing Efficiency of Particles in Heavy Metal Removal Processes under Various Inlet Conditions. *Water* **2019**, *11*, 1135. [[CrossRef](#)]
9. Barai, D.P.; Bhanvase, B.A.; Żyła, G. Experimental Investigation of Thermal Conductivity of Water-Based Fe₃O₄ Nanofluid: An Effect of Ultrasonication Time. *Nanomaterials* **2022**, *12*, 1961. [[CrossRef](#)]
10. Liosis, C.; Papadopoulou, A.; Karvelas, E.; Karakasidis, T.E.; Sarris, I.E. Heavy Metal Adsorption Using Magnetic Nanoparticles for Water Purification: A Critical Review. *Materials* **2021**, *14*, 7500. [[CrossRef](#)]
11. Sindhu, S.; Gireesha, B.J.; Sowmya, G.; Makinde, O.D. Hybrid Nanoliquid Flow through a Microchannel with Particle Shape Factor, Slip and Convective Regime. *Int. J. Numer. Methods Heat Fluid Flow* **2022**, *32*, 3388–3410. [[CrossRef](#)]
12. Serga, V.; Burve, R.; Maiorov, M.; Krumina, A.; Skaudžius, R.; Zarkov, A.; Kareiva, A.; Popov, A.I. Impact of Gadolinium on the Structure and Magnetic Properties of Nanocrystalline Powders of Iron Oxides Produced by the Extraction-Pyrolytic Method. *Materials* **2020**, *13*, 4147. [[CrossRef](#)]
13. Kumar, S.; Nair, R.R.; Pillai, P.B.; Gupta, S.N.; Iyengar, M.A.R.; Sood, A.K. Graphene Oxide-MnFe₂O₄ Magnetic Nanohybrids for Efficient Removal of Lead and Arsenic from Water. *ACS Appl. Mater. Interfaces* **2014**, *6*, 17426–17436. [[CrossRef](#)] [[PubMed](#)]
14. Singh, S.; Barick, K.C.; Bahadur, D. Surface Engineered Magnetic Nanoparticles for Removal of Toxic Metal Ions and Bacterial Pathogens. *J. Hazard. Mater.* **2011**, *192*, 1539–1547. [[CrossRef](#)] [[PubMed](#)]
15. Zhang, X.; Huang, Y.; He, X.; Lin, J.; Yang, X.; Li, D.; Yu, M.; Yu, C.; Tang, C. Synergistic Adsorption of Pb(II) Ions by Fe₃O₄ Nanoparticles-Decorated Porous BN Nanofibers. *Colloids Surf. A Physicochem. Eng. Asp.* **2020**, *589*, 124400. [[CrossRef](#)]
16. Berrehal, H.; Sowmya, G.; Makinde, O.D. Shape Effect of Nanoparticles on MHD Nanofluid Flow over a Stretching Sheet in the Presence of Heat Source/Sink with Entropy Generation. *Int. J. Numer. Methods Heat Fluid Flow* **2021**, *32*, 1643–1663. [[CrossRef](#)]
17. Papadopoulou, A.; Chalmpes, N.; Gournis, D.; Kostopoulou, N.; Efthimiadou, E. Synthesis, Characterization and Evaluation of Aqueous Zn-Based Quantum Dots for Bioapplications. *Dalt. Trans.* **2022**, *51*, 3452–3461. [[CrossRef](#)]
18. Aksimentyeva, O.I.; Savchyn, V.P.; Dyakonov, V.P.; Piechota, S.; Horbenko, Y.Y.; Opainych, I.Y.; Demchenko, P.Y.; Popov, A.; Szymczak, H. Modification of Polymer-Magnetic Nanoparticles by Luminescent and Conducting Substances. *Mol. Cryst. Liq. Cryst.* **2014**, *590*, 35–42. [[CrossRef](#)]
19. Arockiam, S.; Cheng, Y.H.; Armenante, P.M.; Basuray, S. Experimental Determination and Computational Prediction of the Mixing Efficiency of a Simple, Continuous, Serpentine-Channel Microdevice. *Chem. Eng. Res. Des.* **2021**, *167*, 303–317. [[CrossRef](#)]
20. Nguyen, Q.M.; Abouezzi, J.; Ristroph, L. Early Turbulence and Pulsatile Flows Enhance Diodicity of Tesla's Macrofluidic Valve. *Nat. Commun.* **2021**, *12*, 2884. [[CrossRef](#)]
21. Weng, X.; Yan, S.; Zhang, Y.; Liu, J.; Shen, J. Design, Simulation and Experimental Study of a Micromixer Based on Tesla Valve Structure. *Huagong Jinzhan/Chem. Ind. Eng. Prog.* **2021**, *40*, 4173–4178. [[CrossRef](#)]
22. Hossain, S.; Ansari, M.A.; Husain, A.; Kim, K.Y. Analysis and Optimization of a Micromixer with a Modified Tesla Structure. *Chem. Eng. J.* **2010**, *158*, 305–314. [[CrossRef](#)]
23. Wang, C.T.; Chen, Y.M.; Hong, P.A.; Wang, Y.T. Tesla Valves in Micromixers. *Int. J. Chem. React. Eng.* **2014**, *12*, 397–403. [[CrossRef](#)]
24. Bhagat, A.A.S.; Papautsky, I. Enhancing Particle Dispersion in a Passive Planar Micromixer Using Rectangular Obstacles. *J. Micromechanics Microengineering* **2008**, *18*, 085005. [[CrossRef](#)]
25. Yang, A.S.; Chuang, F.C.; Chen, C.K.; Lee, M.H.; Chen, S.W.; Su, T.L.; Yang, Y.C. A High-Performance Micromixer Using Three-Dimensional Tesla Structures for Bio-Applications. *Chem. Eng. J.* **2015**, *263*, 444–451. [[CrossRef](#)]
26. Hong, C.C.; Choi, J.W.; Ahn, C.H. A Novel In-Plane Passive Microfluidic Mixer with Modified Tesla Structures. *Lab Chip* **2004**, *4*, 109–113. [[CrossRef](#)] [[PubMed](#)]
27. Vartholomeos, P.; Mavroidis, C. In Silico Studies of Magnetic Microparticle Aggregations in Fluid Environments for MRI-Guided Drug Delivery. *IEEE Trans. Biomed. Eng.* **2012**, *59*, 3028–3038. [[CrossRef](#)]
28. Teja, A.S.; Koh, P.-Y. Synthesis, Properties, and Applications of Magnetic Iron Oxide Nanoparticles. *Prog. Cryst. Growth Charact. Mater.* **2009**, *55*, 22–45. [[CrossRef](#)]
29. Chicot, D.; Mendoza, J.; Zaoui, A.; Louis, G.; Lepingue, V.; Roudet, F.; Lesage, J. Mechanical Properties of Magnetite (Fe₃O₄), Hematite (α-Fe₂O₃) and Goethite (α-FeO·OH) by Instrumented Indentation and Molecular Dynamics Analysis. *Mater. Chem. Phys.* **2011**, *129*, 862–870. [[CrossRef](#)]
30. Chang, Y.-C.; Chen, D.-H. Preparation and Adsorption Properties of Monodisperse Chitosan-Bound Fe₃O₄ Magnetic Nanoparticles for Removal of Cu(II) Ions. *J. Colloid Interface Sci.* **2005**, *283*, 446–451. [[CrossRef](#)]
31. Zhang, Y.; Ni, S.; Wang, X.; Zhang, W.; Lagerquist, L.; Qin, M.; Willför, S.; Xu, C.; Fatehi, P. Ultrafast Adsorption of Heavy Metal Ions onto Functionalized Lignin-Based Hybrid Magnetic Nanoparticles. *Chem. Eng. J.* **2019**, *372*, 82–91. [[CrossRef](#)]
32. Karvelas, E.; Liosis, C.; Karakasidis, T.; Sarris, I. Micromixing Nanoparticles and Contaminated Water under Different Velocities for Optimum Heavy Metal Ions Adsorption. *Environ. Sci. Proc.* **2020**, *2*, 65. [[CrossRef](#)]

33. Weller, H.G.; Tabor, G.; Jasak, H.; Fureby, C. A Tensorial Approach to Computational Continuum Mechanics Using Object-Oriented Techniques. *Comput. Phys.* **1998**, *12*, 620. [[CrossRef](#)]
34. Ramesha, D.K.; Anvekar, A.; Raj, A.; Vighnesh, J.; Tripathi, S. A DSMC Analysis of Gas Flow in Micro Channels Using OpenFOAM. In Proceedings of the International Conference on Advances in Mechanical Engineering Sciences (ICAMES-17), P.E.S. College of Engineering, Mandya, India, 21–22 April 2017.
35. Su, Y.; Lautenschleger, A.; Chen, G.; Kenig, E.Y. A Numerical Study on Liquid Mixing in Multichannel Micromixers. *Ind. Eng. Chem. Res.* **2014**, *53*, 390–401. [[CrossRef](#)]
36. Ortega-Casanova, J.; Lai, C.H. CFD Study about the Effect of Using Multiple Inlets on the Efficiency of a Micromixer. Assessment of the Optimal Inlet Configuration Working as a Microreactor. *Chem. Eng. Process. Process Intensif.* **2018**, *125*, 163–172. [[CrossRef](#)]
37. Chen, X.; Shen, J. Numerical Analysis of Mixing Behaviors of Two Types of E-Shape Micromixers. *Int. J. Heat Mass Transf.* **2017**, *106*, 593–600. [[CrossRef](#)]
38. Peng, G.; He, Q.; Lu, Y.; Huang, J.; Lin, J.M. Flow Injection Microfluidic Device with On-Line Fluorescent Derivatization for the Determination of Cr(III) and Cr(VI) in Water Samples after Solid Phase Extraction. *Anal. Chim. Acta* **2017**, *955*, 58–66. [[CrossRef](#)]
39. Lok, K.S.; Kwok, Y.C.; Nguyen, N.T. Passive Micromixer for Luminol-Peroxide Chemiluminescence Detection. *Analyst* **2011**, *136*, 2586–2591. [[CrossRef](#)]